CHEMISTRY
A European Journal

A Journal of
ChemPubSoc Europe

Accepted Article

Title: Solution-processable Unsymmetrical Triarylamines: Towards High Mobility and ON/OFF Ratio in Bottom-gated OFET

Authors: Samuthira Nagarajan, Ramachandran Dheepika, Predhanekar Mohamed Imran, and Nattamai S. P. Bhuvanesh

To be cited as: *Chem. Eur. J.* 10.1002/chem.201903450

Link to VoR: http://dx.doi.org/10.1002/chem.201903450

Supported by
ACES

WILEY-VCH

10.1002/chem.201903450

WILEY-VCH

FULL PAPER

Solution-processable Unsymmetrical Triarylamines: Towards High Mobility and ON/OFF Ratio in Bottom-gated OFET

Ramachandran Dheepika,[a] Predhanekar Mohamed Imran,[b] Nattamai S. P. Bhuvanesh,[c] Samuthira Nagarajan*[a]

Abstract: Self-assembly of organic small molecules into an ordered thin film has been the key strategy towards efficient charge transport for organic field-effect transistors (OFETs). Solution processing is witnessed to be a feasible and economic way to enhance *pi-pi* interaction. Here, we report nitrile substituted unsymmetrical triarylamines for OFET applications with high mobility. Molecules are constructed by Suzuki cross-coupling reaction under inert conditions. HOMO level ~5.3 eV indicates good hole transporting ability. OFETs are assembled in bottom gate top contact (BGTC) architecture. Devices fabricated from a binary solvent system exhibited excellent *p*-channel characteristics; with impressively high charge carrier mobility up to 2.58 $cm^2 V^{-1} s^{-1}$ and the $I_{on/off}$ current was $10^6/10^7$. SEM and AFM analysis showed the efficient molecular self-assembly attained by simple, effective solvent engineering method. Theoretical insights obtained by DFT calculation supported by single crystal structures proves the crystalline nature and packing modes of these molecules ensures high mobility. The results prove that these molecules have great potential to be used for numerous electronic applications such as sensors and logic switches.

Introduction

Organic field-effect transistors (OFETs), since the first report in 1986, [1] are becoming significant constituents of electronics, with inherent merits of organic molecules. OFETs can transduce/amplify signals and act as switches thus impressively simplify device structure. [2] Furthermore, because of their light weight, flexibility, low operating voltage, large-scale production at low temperatures OFETs have great potential in various fields. OFETs can be ideally utilized in large displays and radio frequency identification (RFID) tags. In addition, owing to their stability and mechanical flexibility, they are useful in sensors, as electronic watermarks on banknotes, and as wearable electronics. [3] OFETs offer potential benefits for the commercialization of low-cost printing and highly sensitive and selective detection platforms. [4] Non-volatile memory systems with OFETs have been studied for their signal addressing behavior. [5] Prodigious improvements have been made in the fabrication style of devices and the synthesis of proficient organic semiconducting molecules. [6, 7]

Despite these headways, scrutiny of the relationship between molecular interactions (*pi-pi*) and packing styles is very critical to understand charge transport. It has been proved that *pi-pi* interactions can be changed by other molecular interactions such as steric effect of arms, van der Waals forces and coulomb interactions. [8] Charge transport can be fine-tuned by precise molecular engineering; [9] thus, choosing a suitable fabrication style is attracting interest in recent research. [10] To fabricate an active semiconducting layer, vacuum vapor deposition methods and solution-processable methods are competitively employed. However, recent research is concerned more about solution processability as a platform to afford a simplified fabrication. [11, 12]. Spin coating, dip casting, and ink jet printing are ideal examples of solution processing methods. [13] Solution-processed small molecules result in highly crystalline films with low-density grain boundaries. [14] The size and boundary of the grains can be improved by changing the solvent and the processing temperature. Thermal stability of an active semiconducting layer is emerging as an additional requirement for organic transistors.

Triarylamine (TAA)-based organic semiconducting molecules are acknowledged as hole-transporting, electron-donating materials and are used as components in different devices [15] owing to their small reorganization energy (λ) value. Molecules with linear and cyclic architectures are constructed using TAAs are extensively employed in optoelectronic devices due to their good charge transporting and emissive nature. [16] TAAs' peculiar geometrical features will throw light on the structure and property relationship. They have been studied as suitable materials for OFETs in the past two decades. Saragi et al. [17] demonstrated the OFET behavior of thermally evaporated amorphous spiro-linked triphenylamine. However, the devices had good ON/OFF ratio and morphological stability with respect to time and atmosphere, the mobility obtained was very low. Sonntag et al. [18] analyzed the solution-processable OFET properties of molecular glasses formed from star-shaped triphenylamine with carbazole and fluorene side arms. The molecular glasses exhibited very small hysteresis and moderate ON/OFF ratio with low threshold voltage, and the mobility obtained was 10^{-4} $cm^2 s^{-1} V^{-1}$. Wei Xu and co-workers [19] reported a macrocyclic triphenylamine possessing decomposition temperature of 375 °C in their OFET. However, the mobility and ON/OFF ratio were moderate in both solution-processed and vacuum-deposited devices. Antonio Cravino and co-workers [20] prepared triphenylamine-thiophene hybrid systems for optoelectronics applications. They stated that amorphous or glassy films do not require any control of molecular orientation; the devices they fabricated had good mobility but possessed very poor ON/OFF ratio.

[a] Ramachandran Dheepika, Prof. Samuthira Nagarajan*
Department of Chemistry
Central University of Tamil Nadu,
Thiruvarur- 610 005, India
E-mail: snagarajn@cutn.ac.in
[b] Dr. Predhanekar Mohamed Imran
Department of Chemistry,
Islamiah College,
Vaniyambadi - 635 752, India
[c] Dr. Nattamai S. P. Bhuvanesh
Department of Chemistry,
Texas A &M University,
TX77842, USA

10.1002/chem.201903450

In our recent communication, [21] we reported the first unsymmetrical TAAs for OFET applications. In this study, to further investigate stability and device efficiency, we have synthesized a series of relatively stable new nitrile-substituted unsymmetrical TAAs. TAA molecules are designed with highly conjugated aryl substituents in two arms and third arm with electron withdrawing CN group, thus electron distribution over molecule will be modified. CN group is introduced to alter twist and tilt angle in triarylamine moiety to reach an unsymmetrical structure. It is expected that the unsymmetrical functionalization of TAA will stimulate an efficient self-assembly to produce uniform thin film and will result in improved mobility.

Results and Discussion

Here, we report on OFETs with a series of differently and unsymmetrically substituted triarylamines. In addition, we show that the suitably substituted TAAs influence the charge carrier mobility due to crystalline nature of the thin film. TAAs are functionalized with an electron-withdrawing CN substituent to the pi- extended triarylamine moiety that can lower the molecular orbital energy level [22] and can facilitate charge injection. An unsymmetrical structure is expected to give rise to more twist in the molecule and an efficient molecular self-assembly to attain higher charge carrier mobility. Introduction of electron-withdrawing (-NO_2 and -CF_3) and electron-donating substituents (-OCH_3 and thiophene) alters the frontier molecular orbital's position and tunes the bandgap. The schematic to synthesize the target molecules is represented in **Scheme 1**. The compounds **2-8** were constructed by Suzuki cross-coupling reaction from iodinated triarylamine nitrile under inert conditions.

2.1 Photophysical properties

To elucidate the optoelectrical properties, UV-vis absorption spectra of the synthesized compounds were analyzed in anhydrous dichloromethane at 10^{-5} M concentration. The spectra and data are represented in **Figure. 1a** and **Table 1** respectively. Molecules first exhibit two bands around 260 nm to 280 nm attributed to π-π* transition, followed by a more pronounced band around the wavelength of 350 nm; the absorption maximum (λ_{max}) corresponds to n-π* transition. Comparison of optical data of compounds **2-8** with the precursor **1** proves that the introduction of a new aryl group with electron donating and electron withdrawing groups alters the photophysical behavior of TAAs remarkably. [27] Molecule **4** has the maximum absorption with red shift due to the incorporation of highly conjugated biphenyl unit in two arms. Compound **3** has an extension of naphthalene units and gives a 12 nm bathochromic shift from **2** with similar π-π* transition. On the other hand, presence of electron-withdrawing groups NO_2 and CF_3 (**7** and **8**) also results in bathochromic shift compared to electron-donating thiophene and OCH_3 groups. Molecule **5** covers a broad region of 123 nm in the UV-vis spectrum from 282 nm to 405 nm due to annexation of thiophene rings, and it has the second highest absorption coefficient (ε). Similarly, electron withdrawing, chromophoric NO_2 substitution also gave good ε value. [28] Molecule **1**, which has very less conjugation when compared

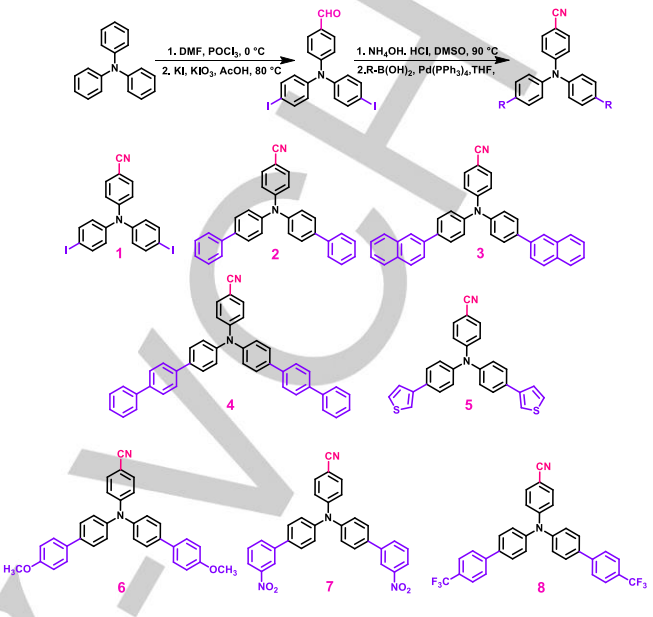

Scheme 1. Synthetic route and structure of compounds **1-8**

with the other molecules, has the lowest absorption coefficient. Fluorescence spectra of the compounds **1-8** at the concentration of 10^{-8} M were obtained in anhydrous dichloromethane. **Figure 1b** shows the spectra, and the values are given in **Table 1**. The pattern in the spectra clearly shows that the excited state of all the molecules have changed drastically from ground state.

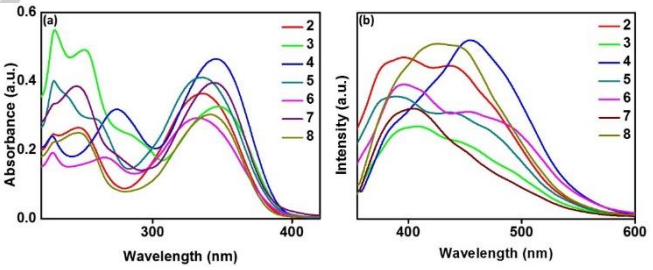

Figure 1. (a) Absorption and (b) emission spectra of compounds **1-8**

Although these molecules attain significant dipole moment in a relaxed excited state, molecule twisting is deceptively decoupled from the charge transfer without the help of solvent. [27] In the excited state, excitons are localized in any one of the arms with respect to different conformational changes in the excited states. [29] So emission spectra of all the new functionalized TAAs are not observed as a single sharp peak. Extension in conjugation in molecule **3** is restricted within the naphthalene unit as they are in different planes from the center core moiety. [28, 29] Compound **3** has the lowest intensity when compared with the other molecules.

The extension of conjugative delocalization in molecule **4** dictates the maximum shift, 66 nm towards higher wavelength with respect to biphenyl substitution. The twisted side arm results in a different spectrum pattern when compared with the other molecules. Molecules **7** and **8** have a single but broad peak, which may be due to the electron-withdrawing behavior of the substituents.

Table 1. . Photophysical properties of the synthesised compounds **1**-**8**

Compd. No.	λ_{abs} (nm)		λ_{em} (nm)	Stokes shift(nm)	Absorption coefficient, ε (10^4 M^{-1} cm^{-1})
	λ_1	λ_{max}			
1	318	335	407	72	2.4
2	246	334	408	74	3.7
3	251	346	451	105	3.3
4	274	346	454	108	4.7
5	259	334	456	122	4.1
6	265	332	458	126	2.9
7	245	344	456	112	3.9
8	246	341	445	104	3.0

Absorption and emission spectra of compounds **1**-**8** in coated thin films are presented in **Figure S1** and **S2**. Compared with the solution state, spectra are broad and shifted to higher wavelengths. It is attention-grabbing that the pattern of the spectra and electronic transitions are almost similar for all compounds. The edge of the absorption spectra is greatly shifted from the UV region to the visible region (200-500 nm). This bathochromic shift was observed in the emission spectra as well. However, compounds **4** and **8** have hypsochromic shift, which may be due to different structural alignments in the excited state. Noticeably, compound **8** shows an additional peak at higher wavelength (510 nm). This shoulder peak can be accounted for the enhanced vibronic splitting in solid thin films. [41]

2.2 Electrochemical properties

Cyclic voltammetry is a prevailing technique employed to elucidate the electronic energy level of molecules. Cyclic voltammograms are shown in **Figure 2**, and the values are given in **Table 2**. The CV curves remain unchanged after multiple scans. A conventional three-electrode cell setup was used with glassy carbon as the working electrode, platinum wire as the counter-electrode, and a standard calomel electrode as the reference. The system was standardized externally using Fc/Fc+. Molecules were analyzed in anhydrous acetonitrile (10^{-5} M) with tetrabutylammonium hexafluorophosphate (0.1 M) as the supporting electrolyte at a scan rate of 50 mV/s. All the electron-transfer reactions are irreversible, and nitro-substituted **7** shows an additional peak in the negative potential. TAA possesses a multistep electrochemical process. [30] One of the noticeable electrochemical behaviors of TAAs is oxidizability of the central nitrogen atom. They can efficiently transport positive charges by radical cations. [30] Compound **1** possesses a high oxidation potential (1.04 eV). The oxidation potentials of the molecules fall in the range of 0.75 to 1.01 eV. E_{ox} values vary depending on the electron-withdrawing and electron-donating substituents. The oxidation observed around 0.75 to 1 eV corresponds to the triphenylamine core. These oxidation potential values were used to estimate the HOMO levels of the compounds. The potential values are estimated against standard calomel electrode (SCE). HOMO values were calculated using the formula E_{HOMO} = - (E_{ox} + 4.8 - $E_{Fc/Fc+}$). [31] $E_{1/2}$ of the Fc/Fc^+ redox couple measured was 0.4 eV in the presence of supporting electrolyte. The calculated HOMO values are given in **Table 2.** LUMO values were obtained from the optical band gaps.

Voltammograms show that functionalizing compound **1** with various substituents result in altered HOMO levels, ranging from 5.2 to 5.5 eV. The LUMO level was lowered to 2.3 eV for

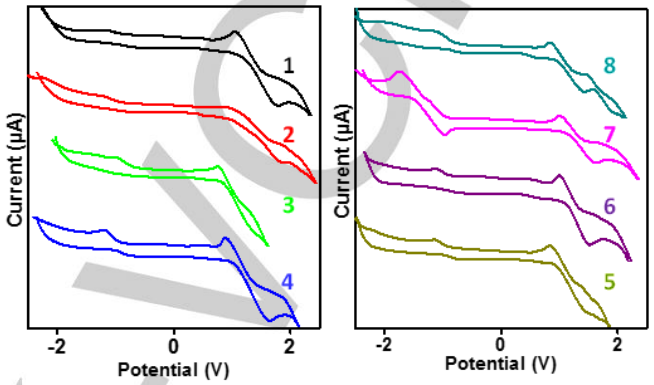

Figure 2. Cyclic voltammograms of compounds **1**-**8**

Table 2. . HOMO, LUMO and band gap values of compounds **1**-**8**

C. No	E_{ox} eV	Experimental (eV)			Computational (eV)		
		HOMO	LUMO	Band gap	HOMO	LUMO	Band gap
1	1.04	-5.53	-2.25	3.28	-5.77	-1.80	3.97
2	0.89	-5.38	-2.21	3.17	-5.28	-1.43	3.85
3	0.93	-5.42	-2.35	3.00	-5.24	-1.51	3.73
4	0.75	-5.24	-2.06	3.18	-5.52	-1.71	3.81
5	0.85	-5.34	-2.55	3.20	-5.36	-1.34	4.02
6	0.84	-5.33	-2.12	3.21	-5.14	-1.27	3.87
7	1.01	-5.50	-2.26	3.24	-5.73	-2.80	2.93
8	0.99	-5.49	-2.30	3.19	-5.64	-1.80	3.85

compound **1**. Indeed, electron-donating thiophene, and methoxyphenyl groups lead to easier oxidation than the electron-withdrawing nitrophenyl and trifluorophenyl groups and result in a slight cathodic shift. In the first scan in the anodic range in all compounds (Except **7**), a single peak is obtained, which was shifted to a less positive value when compared with **1**. LUMO levels lowered to 2.3 eV, indicating that the electron injection barriers of these molecules are reduced. [32] Noticeably, compound **5** has a higher LUMO value because of the electron-donating nature of the substituted thiophene. Compounds **2** and **4** retain almost the same band gap values, whereas **3** shows the lowest bandgap, which may be due to the naphthyl units, which have increased conjugation by the linear annulation of phenyl rings and result in improved and uniform electron delocalization. [33] In compound **4**, due to the impact of molecular twisting of the adjacent phenyl rings, the electronic effect of increasing π delocalization band gap matches with that in compound **2**. LUMO of compounds **7** and **8** are located over the side arms with NO_2 and CF_3 phenyl substitution (Figure **8**). Interestingly, compound **7** shows an additional irreversible redox peak in negative potential, which may be due to the presence of two nitro groups. Electron

10.1002/chem.201903450

withdrawing nature of these substituents shift the oxidation potential to 1.01 and 0.99 eV respectively (on comparison with compound 2 with E_{ox} 0.89 eV).

2.3 Thermal Behaviour

The thermogravimetric analysis (TGA) and differential scanning calorimetry (DSC) methods were employed to analyze thermal behavior of the molecules. In TGA, scan from 25 °C to 800 °C at 5°C min^{-1} in nitrogen atmosphere revealed the thermal stability of the new triarylamines. DSC thermograms and TGA curved are presented in **Figure 3** and **4** respectively. DSC scans were carried out in nitrogen atmosphere at 10°C/min. Thermal stability of molecules play an important role in device fabrication, efficiency, and lifetime of the fabricated devices. Glass transition temperature (T_g) for the compounds **2**-**4**, **7** and **8** are in the range of 111-158 °C. Melting points (T_m) were observed as sharp

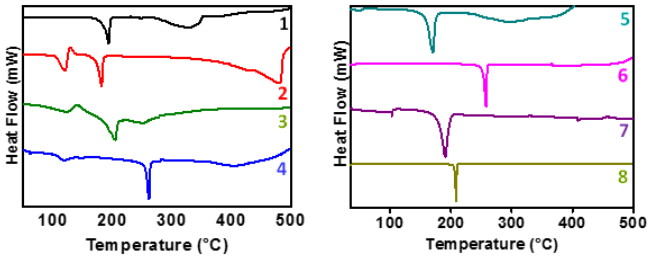

Figure 3. Differential scanning calorimetry thermogram of compounds **1**-**8**

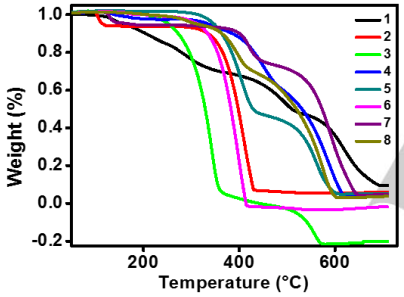

Figure 4. Thermogravimetric curves of compounds **1**-**8**

endothermic peaks. Molecule **4** had the highest melting point at 261°C; similarly, compound **6** also had a melting point of 257 °C. All the molecules had melting points higher than 150 °C. TAA-based hole transporting materials were analyzed by Robertson et al. [34] wherein the melting points ranged from 120 to 160 °C.

Table 3. Thermal behaviour of compounds **2**-8

Compd. No.	T_g °C	T_m °C	T_d °C
2	111	180	345
3	136	204	516
4	131	261	512
5	-	170	520
6	257	330	330
7	191	530	530
8	208	497	497

Krucaite and co-workers [35] have reported about naphthalene substituted TAA for PhOLEDs with a melting temperature of ~150°C. From TGA curves it is observed that all the compounds have decomposition points (T_d) ranging from 408 – 633 °C at 10 % weight loss (**Table 3**). Many triarylamine-based hole transporting materials have been reported with moderate melting and decomposition points. [36] In our previous work, [21] we have reported formyl functionalized TAA molecules with relatively good thermal stability. Replacing the formyl group with nitrile group remarkably improved the thermal behavior of the compounds. These nitrile molecules have promoted thermal stability and guarantees the durability of device. Values extracted from TGA and DSC are provided in **Table 3**.

2.4 Single crystal X-ray crystallography

A Quest X-ray (fixed-Chi geometry) diffractometer was used for screening of crystals, unit cell determination, and data collection. The X-ray radiation was generated from a Mo-Iμs X-ray tube (K = 0.71073 Å). Colorless crystals of compounds **2** and **6** were obtained by slow evaporation of their dichloromethane and methanol solutions. Thermal ellipsoid plots are shown in **Figure 5** and **6** with atomic labelling. Compound **2** crystalized in triclinic form with P-1 space group, and compound **6** crystalized in monoclinic form with P 1 21/c 1 space group

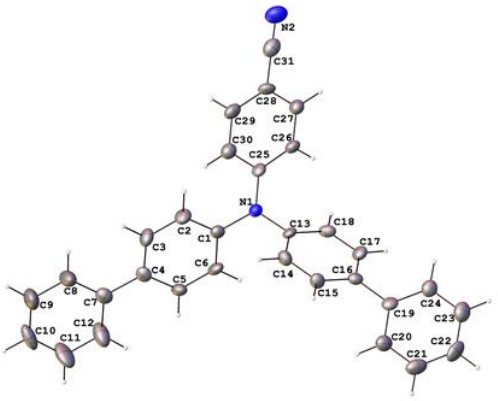

Figure 5. Thermal ellipsoid plot of compound **2**

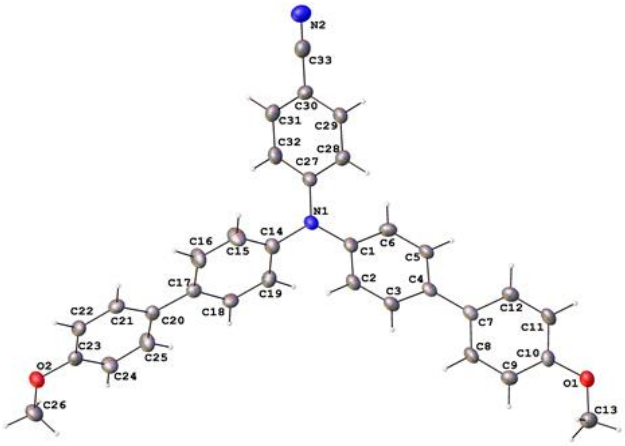

Figure 6. Thermal ellipsoid plot of compound **6**

2.5 Morphological Studies

10.1002/chem.201903450

Morphology of active thin films of the devices (five devices, with compounds **3**-**6** and **8**) was examined by SEM and AFM techniques. **Figure 7** shows SEM images of thin films formed by spin coating of compounds after baking at 80 °C. AFM images are shown in **Figure S3** in supporting information. All the compounds resulted in an ordered thin film.

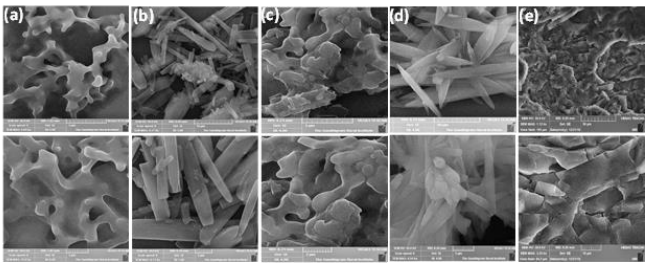

Figure 7. SEM images of compounds (a) **3**, (b) **4** (c) **5**, (d) **6**, (e) **8**

From SEM analysis, compound **3** and **5** shows spindle fiber and coral network respectively. Other two compounds (**4**, and **6**) shows crystalline network. Compound **8** exhibits large quadrant arrangement. This consistent microstructural architecture of the solid thin films ensures efficient charge carrier movement.

2.6 Computational basis

To understand the Fermi level of the molecules, density of states (DOS) calculations were performed using the PBE functional method. To construct polycrystals, MedeA software was used from the single-crystal level. Initially, dimers were constructed to measure the interactive distance and the polycrystalline nature of the molecules. At the DFT-PBE-GGA level of theory, optimized molecule structure was processed through MedeA software to predict the crystal structures, and crystalline packing. (Details in supporting information). The optimized molecular structure of the molecules (**Figure S5**) were generated by using (B3LYP/6-31G (d)) density functional theory, and they have been examined for geometrical and electronic features in ground state systematically. In triarylamines, the central nitrogen atom shows significant contribution in the HOMO level, where the LUMO will be located over the acceptor moiety. **Figure. 8** shows qualitative representation of FMOs of molecules **1**-**8**. From the analysis of all the HOMO and LUMO of the molecules, it is inferred that all the molecules have a very high percentage of HOMO on the main moiety and low percentage over the substituents. LUMO is spread over the acceptor moiety. Molecules **1**-**6** have LUMO on nitrile-substituted arm, but molecules **7** and **8** exhibit a remarkable distribution. The introduction of strong electron-withdrawing NO_2 and CF_3 groups in the substituents changes the distribution. Meta-substitution of the nitro group has shown a difference in electron delocalization from the para substituted CF_3 group; in molecule **7**, the nitro phenyl ring only holds the LUMO distribution, whereas in molecule **8**, the complete arms from the central nitrogen clutches the distribution. All the space groups from the Cambridge structural database reference were tried sequentially and packing measurements were obtained. Molecules possessing ideal packing at optimal lattice distances were studied. The optimized geometry was fed to MedeA, which further predicted the crystal pattern of each molecule using the VASP software at the DFT-PBE-GGA level (**Figure S7** and **S8**, Supporting information). The crystal parameters are in good agreement with the single-crystal XRD data.

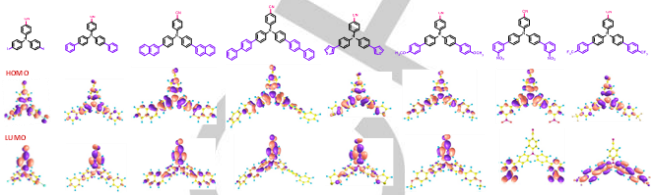

Figure 8. Qualitative representation of FMOs of molecules **1-8**

.

2.7 OFET characteristics

OFET devices were fabricated in BGTC architecture. Active layer was incorporated into the device plan by spin coating. The molecule in a binary solvent mixture, which is comprised of toluene and chloroform in 7:3 ratio was spun on the dielectric layer. The lower surface tension of low boiling solvent such as chloroform will provide a well ordered film on substrate. And removal of residual solvents by thermal annealing will not disturb the self-assembly. In addition, introducing relatively high boiling solvent toluene in deposition process, regulates the evaporation speed and prevents amorphous packing in film. And also they provide adequate time for the molecules to self-assemble by inter and intramolecular interactions. Among all the synthesised compounds, only five (**3**-**6** and **8)** showed OFET characteristics. The output and transfer characteristic curves are given in **Figure 9**. Values extracted from the graphs are provided in **Table 4**. The threshold voltage (V_{TH}) and charge carrier mobility (μ) were calculated from the intercept and slope of the linear plot of the square root of drain to source current ($I_{DS}^{1/2}$) versus the gate voltage. The following formula [37] was used to calculate charge carrier mobility from the saturation regime

$$\mu = \frac{2L}{CW}\,(Slope)^2$$

Where, C is capacitance of the dielectric layer per unit area, L and W are length and width of the channel, respectively. Compounds **3**, **4**, **5**, and **8** have very good ON/OFF current ratio, 10^7, 10^6, 10^6, and 10^7 respectively, whereas compound **5** has an $I_{ON/OFF}$ ratio of 10^4. This high ON/OFF ratio of the devices is noteworthy for improved performance and minimized leakage. These values ensured a well-defined gate contact in the bottom gate top contact architecture. Devices with high $I_{ON/OFF}$ can be potentially utilized in switches, logic circuits, memory devices, and various sensors. [38] All of them possess a very good charge carrier mobility (**Table 4**).

10.1002/chem.201903450

Among the five compounds, compound **3** has excellent carrier mobility, up to 2.58 $cm^2 V^{-1} s^{-1}$; the highest of the earlier reported values. By controlling the active layer's thickness, the pinch-off voltage may be minimized and results in improved ON/OFF ratio in the devices. [39] This can be substantiated by the excellent intermolecular interaction of the naphthalene units substituted in

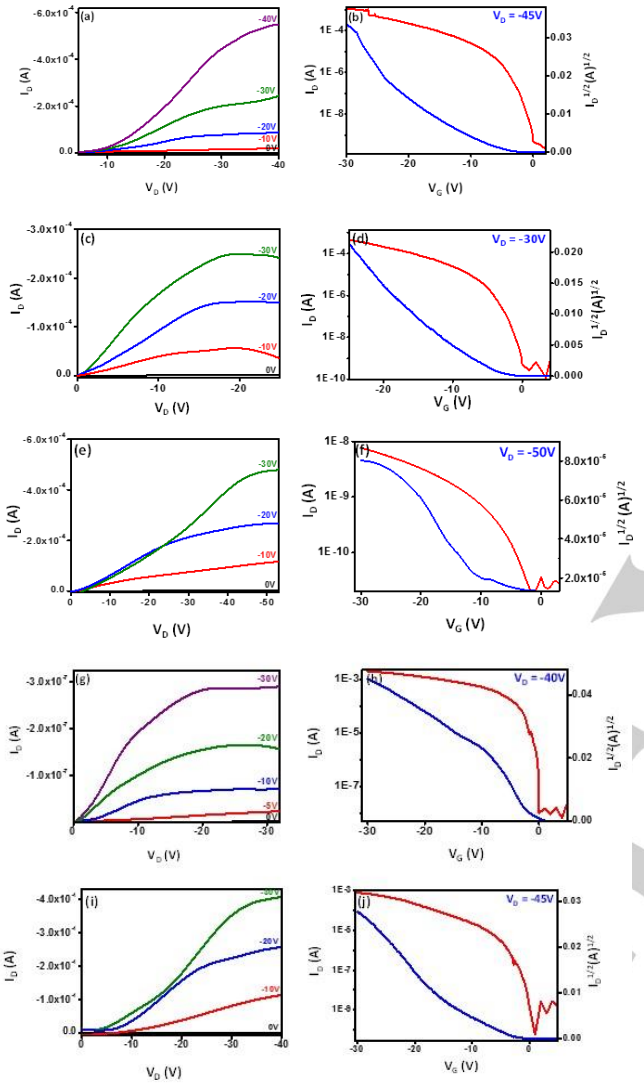

Figure 9. OFET characteristic curves of BGTC devices made of compounds **3** (a, b), **4** (c, d), **5** (e, f), **6** (g, h), and **8** (i, j)

the side arms. Compound **3** has a better crystal parameters, and the packing shows efficient pi-pi stacking (**Figure S7** and **S8**, Supporting information). The interatomic distances between the central nitrogen atom and the phenyl hydrogen atoms are 5.8 Å and 6.7Å; this facilitates better charge carrier passage. The crystal lattice parameters are given in Table **S3** (Supporting information). The efficient molecular self-assembly of these molecules in casted thin film provides good mobility. Compound **6** and **8** exhibited unalike threshold voltage; the value was calculated considering the up/downward kink [33] observed in the transfer characteristics. All these results are upgraded from previously reported values. [20, 21] The charge carrier mobility was improved from the other cyclic and starburst molecules reported, [17-19] with 10^{-3} and 10^{-4} $cm^2 V^{-1} s^{-1}$ mobility. ON/OFF ratio is also improved to 10^7, and the threshold voltage was minimized noticeably. Fused rings will possess comparatively low reorganization energy than any other π extensions. Owing to this property, Compound **3** shows exceptionally virtuous OFET characteristics. Charge carrier mobility of the device is the most imperative parameter for many targeted applications such as displays and RFIDs.

Table 4. OFET characteristics of compounds **3-6** and **8**

Compd. No.	Mobility ($cm^2 V^{-1} s^{-1}$)	V_{TH}(V)	$I_{on/off}$
3	2.58	-6	10^7
4	0.25	-4	10^6
5	0.66	-10	10^4
6	0.41	-1[a]	10^6
8	0.87	-2[a]	10^7

[a] Calculated by considering the kink [33] observed in the $I_D^{1/2}$ curve in transfer characteristics

Conclusions

In summary, solution processable OFETs with high performance have been proposed based on nitrile-substituted unsymmetrical triarylamines (TAAs). The designed molecules were synthesized via Suzuki cross-coupling reactions and explored by their optoelectronic, thermal, and electrochemical behaviors. OFETs in bottom gate top contact architecture exhibited *p-type* behavior. Spin coating from a binary solvent system (toluene and chloroform) resulted in crystalline thin film. Thermal annealing process (post deposition) ensures highly ordered thin films with less grain boundaries. These OFETs have remarkably high charge carrier mobility up to 2.58 $cm^2 V^{-1} s^{-1}$, and the $I_{ON/OFF}$ current was $10^6/10^7$. Compound **3** had better crystalline parameters and its packing showed efficient π-π stacking. The interatomic distances between the central nitrogen atom and the phenyl hydrogen atom are 5.8 Å and 6.7 Å, which facilitated efficient mobility. These devices can be potentially employed in active matrix displays, health monitoring devices, memory devices and sensors. These findings can encourage to invent high performing, solution processable, small molecules for electronic applications.

Experimental Section

Materials and Methods

Triphenylamine, all the boronic acids (benzeneboronic acid, naphthylboronic acid, biphenylboronic acid, thiophene-3-boronic acid, 4-methoxyphenylboronic acid, 3-nitrophenylboronic acid, and 4-trifluoromethylboronic acid), $POCl_3$, hydroxylamine hydrochloride, and tetrakis (triphenylphosphine) palladium were used as purchased. N,N-Dimethylformamide (DMF), dimethyl sulphoxide (DMSO), and triethylamine used were anhydrous. All the other solvents (AR grade) were used as received from the commercial sources.

Nuclear magnetic resonance spectra (^{1}H NMR and ^{13}C NMR) were recorded in a Bruker 400 MHz spectrometer in $CDCl_3$. UV-vis absorption spectra were measured using a JASCO UV-NIR spectrophotometer. Fluorescence spectra of the compounds were obtained using the Perkin Elmer Fluorescence spectrometer LS-55. Electrochemical studies were done with CH 6035D Electrochemical Workstation. High-resolution mass spectra were recorded in ThermoExactivePlus UHPLC-MS. Thermal studies were carried out under nitrogen atmosphere in a TA thermal analyzer. Single-crystal X-ray crystallographic data of the crystals were obtained using a Quest X-ray (fixed-Chi geometry) diffractometer. Density functional theory was utilized to analyze the ground-state properties of extended π conjugated systems (VASP ab initio software under MedeA package). The efficiency of compounds was determined by the application of charge transfer integrals calculated with the unique fragment-based approach in Amsterdam Density Functional. [23]The energy dimers Hamiltonian model calculation using ADF software provides the intermolecular electronic coupling. [24] In addition, time-dependent density functional theory (TD-DFT) was also utilized to elucidate excited states.

Synthesis of Compounds 1-8

Compound **1** was prepared using a three-step synthetic sequence from the commercially available triphenylamine (TPA) (**Scheme 1**). Pd-catalyzed Suzuki coupling reactions were performed to synthesize the desired products.

4-(Bis(4-iodophenyl)amino)benzonitrile 1

(a) Vilsmeier-Haack formylation: Compound **1** was synthesized according to the literature. [25] Phosphorus oxychloride (1.85 mL, 20 mmol) was added dropwise to DMF (5.6 mL, 73 mmol) at 0°C and this solution was stirred for 1 hour under the same conditions. To this triphenylamine (5 g, 20 mmol) was added, and the temperature raised to 80°C. After 4 hours, the viscous crude was cooled to room temperature and poured into ice water. The crude was neutralized by 20 % aqueous NaOH. The resultant yellow-colored product was washed with water and extracted with DCM and finally dried over anhydrous Na_2SO_4. The product was purified by column chromatography using an ethyl acetate and hexane gradient system. The product N, N-Di-(4-formylphenyl)aniline, was obtained as pale yellow solid (4.8 g, 88 %).

(b) Iodination: N,N-Di-(4-formylphenyl)aniline (2.5 g, 9.2 mmol) was dissolved in 10 mL of glacial acetic acid; KI (2 g, 11.9 mmol) and KIO_3 (1.91 g, 9.2 mmol) were added and the reaction mixture was stirred at 80°C for 3 hours. After completion, the reaction was quenched with water and cooled to room temperature. The resultant brown-yellow precipitate (4.45 g, 92 %) was filtered under pressure and washed with plenty of water to remove excess of acetic acid.

(c) Triarylamine aldehyde from the previous step was converted into triarylamine nitrile using the method reported. [26] A 100 mL round-bottomed flask was charged with a mixture of N, N-di-(4-formylphenyl)-4-iodoaniline (1.5 g, 3.5 mmol) and hydroxylamine hydrochloride (0.61 g, 8.7 mmol) in DMSO (8 mL). The mixture was stirred at 80°C for 4 hours. The progress of the reaction was monitored by TLC. After completion, the reaction mixture was quenched with water and extracted with dichloromethane. The organic phase was dried over anhydrous Na_2SO_4, and the solvent was removed under reduced pressure. The crude product was further purified by column chromatography to afford 1.3 g of 4-(bis(4-iodophenyl)amino)benzonitrile 1 as a pale yellow powder (88 %)

General Procedure for Suzuki Coupling Reaction

A 100 mL flask was charged with 4-(bis(4- iodophenyl)amino)benzonitrile 1 (500 mg, 0.95 mmol) in anhydrous THF and 10 mol% of $Pd(PPh_3)_4$ in nitrogen atmosphere at room temperature and stirred for 20 minutes followed by the addition of 2 M aqueous Na_2CO_3. Then the corresponding boronic acid (2 mmol) was added and the temperature was raised to reflux. The reaction continued for 7 hours and was monitored by TLC. The crude reaction mixture was cooled to room temperature and the solvent removed under vacuum. The remaining residue was extracted with DCM and washed thrice with distilled water and once with brine solution. The combined organic layer was dried over anhydrous Na_2SO_4 and purified by column chromatography (SiO_2) in a hexane-ethyl acetate gradient system.

Device Fabrication

In this study, we chose an architecture that allows simple fabrication by solution processing-bottom gate top contact (BGTC). In the bottom contact architecture, orientation of the active layer on the S/D (source/drain) electrode varies from that of the dielectric layer. The top contact architecture ensures no discontinuities, as the active layer is entirely coated over the dielectric. Hence, minimum contact resistance is ensured in BGTC architecture. An *n*++ doped silicon (Si) wafer with thermally grown SiO_2 of thickness ~300 nm was used as substrate. The Si substrate was pre-cleaned in acetone and methanol successively, followed by mild base piranha cleaning and washed several times with distilled water. The active layer was incorporated into the device architecture by spin coating from the solution. Solutions were made in a binary solvent system composed of toluene and chloroform in a 7:3 ratio. This combination of solvents resulted in uniform and continuous films. This solution was spun on the substrate at 1800 rpm for 45 seconds. The substrate was then soft baked over a hot plate at 80°C to remove the residual solvent for 45 minutes and followed by annealing at 140°C for an hour. To complete device construction, silver source (S) and drain (D) electrodes were deposited through a mask with channel length of 150 µm and width of 5 mm. The Si wafer acts as gate electrode. Electrical parameters were extracted using a Keithley 4200 SCS semiconductor parameter analyzer system.

Supporting Information

Supporting Information is available from the Wiley Online Library or from the author.

[CCDC 1876639 and 1876640 contains the supplementary crystallographic data for this paper. These data can be obtained free of charge from The Cambridge Crystallographic Data Centre via www.ccdc.cam.ac.uk/data_request/cif.

Acknowledgements

(Financial assistance provided by the Council of Scientific & Industrial Research, New Delhi (02(0222)/14/EMR-II) is gratefully acknowledged. One of the authors (RD) thanks the Central University of Tamil Nadu for a research fellowship.

Keywords: Organic filed-effect transistors • binary solvent system • molecular packing • triarylamines

References

[1] A. Tsumura, H. Koezuka, T. Ando, *Appl. Phys. Lett*., **1986**, *49* (18) 1210.

[2] X. Wu, S. Mao, J. Chen, J. Huang, *Adv. Mater.* **2018**, 1705642.

[3] (a) H. J. Kim, A. Thukral, S. Sharma, C. Yu, *Adv. Mater. Technol*. **2018**, *3*, 1800043 (b) F. A. Viola, A. Spanu, P. C. Ricci, A. Bonfglio, P. Cosseddu, *Sci. Rep*. **2018**, *8*, 8073. (c) A. A. Trul, A. S. Sizov, V. P. Chekusova, O. V. Borshchev, E. V. Agina, M.A. Shcherbina, A. V. Bakirov, S. N. Chvalun, S. A. Ponomarenko, *J. Mater. Chem. C.,* **2018**, *6*, 9649. (d) J. Aimi , P. H. Wang, C.C. Shih, C. F. Huang, T. Nakanishi, M. Takeuchi, H. Y. Hsueh, W. C. Chen, *J. Mater. Chem. C* , **2018**, *6*, 2724. (e) Z. Yin, M. J. Yin, Z. Liu, Y. Zhang, A. P. Zhang, Q. Zheng, *Adv. Sci*. **2018**, *5*, 1701041. (f) X. Ren, F. Yang, X. Gao, S. Cheng, X. Zhang, H. Dong, W. Hu, *Adv. Energy Mater.* **2018**, *8*, 1801003. (g) S. E. Root, S. Savagatrup, A. D. Printz, D. Rodriquez, D. J. Lipomi, *Chem. Rev*., **2017**, *117*, 6467. (h) Y. Liu, M. Pharr, G. A. Salvatore, *ACS Nano*., **2017**, *11*, 9614.

[4] (a) G. Scheiblin, R. Coppard, R. M. Owens, P. Mailley,G. G. Malliaras *Adv. Mater. Technol*. **2017**, *2*, 1600141 (b) C. Zhang, P. Chen, W. Hu, *Chem. Soc. Rev.,* **2015**, *44,* 2087. (c) S. Mun, Y. Park, Y. E. K. Lee, M. M. Sung, *Langmuir,* **2017**, *33*, 13554. (d) X. Wu, S. Mao, J. Chen, J. Huang, *Adv. Mater*. **2018**, *30*, 1705642. (e) C. Zhang, P. Chen, W. Hu, *Chem. Soc. Rev*., **2015**, *44*, 2087. (f) J. Li, R. Bao, J. Tao Y. Peng, C. Pan, *J. Mater. Chem. C*, **2018**, *6*, 11878 (g) H. He, H. Zeng, Y. Fu, W. Han, Y. Dai, L. Xing, Y. Zhang, X. Xue, *J. Mater. Chem. C.,* **2018,** *6*, 9624.

[5] (a) Y. H. Chou,H. J. Yen, C. L. Tsai, W. Y. Lee, G. S. Liou , W. C. Chen *J. Mater. Chem. C*, **2013**, *1* , 3235.(b) W. L. Leong, N. Mathews, B. Tan, S. Vaidyanathan, F. Dotz, S. Mhaisalkar, *J. Mater. Chem.*, **2011**, *21*, 8971. (c) L. Song, Y. Wang, Q. Gao, Y. Guo, Q. Wang, J. Qian, S. Jiang, B. Wu, X. Wang, Y. Shi, Y. Zheng, Y. Li, *ACS Appl. Mater. Interfaces*, **2017**, *9*, 18127.

[6] (a) J. T. E. Quinn, J. Zhu, X. Li, J. Wang and Y. Li, *J. Mater. Chem. C*, **2017**, *5*, 8654-8681. (b) L. Torsi, M. Magliulo, K. Manoli, G. Palazzo, *Chem. Soc. Rev.*, **2013**, 42, 8612. (c) Y. Zhanga, I. Murtazab, and H. Meng, *J. Mater. Chem. C,* **2018,** *6*, 3514.

[7] H. Sirringhaus*, Adv. Mater.* **2014**, *26,* 1319.

[8] (a) A. N. Lakshminarayana, A. Ong, C. Chi, *J. Mater. Chem. C*, **2018**, 6, 3551. (b) C. Sutton, C. Risko, J. L. Bredas, *Chem. Mater.,* **2016**, *28*, 3 (c) J. E. Anthony, J. S. Brooks, D. L. Eaton, S. R. Parkin, *J. Am. Chem. Soc*. **2001,** *123*, 9482. (d) J. H. Dou, Y. Q. Zheng, Z. F. Yao, Z. A. Yu, T. Lei, X. Shen, X. Y. Luo, J. Sun, S. D. Zhang, Y. F. Ding, G. Han, Y. Yi, J. Y. Wang, J. Pei, *J. Am. Chem. Soc*., **2015**, *137*, 15947.

[9] (a) L. Song, Y. Wang, Q. Gao, Y. Guo, Q. Wang, J. Qian, S. Jiang, B. Wu, X. Wang, Y. Shi, Y. Zheng, Y. Li, *ACS Appl. Mater. Interfaces*, **2017**, *9*, 18127. (b) Y. F. Huang, S. T. Chang, K. Y. Wu, S. L. Wu, G. T. Ciou, C. Y. Chen, C. L. Liu, C. L. Wang, *ACS Appl. Mater. Interfaces*, **2018**, *10*, 8869.

[10] (a) S. Tong, J. Sun, J. Yang, *ACS Appl. Mater. Interfaces*, **2018**, *10*, 25902 (b) G. Mattana, A. Loi, M. Woytasik, M. Barbaro, V. Noël, B. Piro *Adv. Mater. Technol*. **2017**, *2*, 1700063 (c). P. J. Diemer, A. F. Harper, M. R. Niazi, A. J. Petty, J. E. Anthony, A. Amassian, O. D. Jurchescu, *Adv. Mater. Technol*. **2017**, *2*, 1700167.

[11] (a) S. Conti, S. Lai, P. Cosseddu, A. Bonfilio, *Adv. Mater. Technol*. **2017**, *2*, 1600212
(b) J. Qian, S. Jiang, S. Li, X. Wang, Y. Shi, Y. Li *Adv. Mater. Technol*. **2018,** 1800182. (c) H. T. Yi, M. M. Payne, J. E. Anthony, and V. Podzorov, Nature Communications, 2012, 3, 125. (d) S. Allard, M. Forster, B. Souharce, H. Thiem, U. Scherf, *Angew. Chem. Int. Ed.* **2008**, *47*, 4070.

[12] T. Matsushima, A. S. D. Sandanayaka, Y. Esaki, C. Adachi, *Sci. Rep*. **2015**, *5*, 14547.

[13] (a) D. Y. Guo, Y. Tsai, T. F. Yu, W. Y. Lee, *J. Mater. Chem. C*, **2018**, *6*, 12006. (b) S. Nam, Y. J. Jeong, J. Jung, S. H. Kim, J. Ahn, K. Shin, J. Jang, *J. Mater. Chem. C,* **2018**, *6*, 799. (c) S. Conti, S. Lai, P. Cosseddu, A. Bonfilio*, Adv. Mater. Technol*., **2017**, *2*, 1600212. (d) Y. Yuan, G. Giri, A. L. Ayzner, A. P. Zoombelt, S. C. B. Mannsfeld, J. Chen, D. Nordlund, M. F. Toney, J. Huang, Z. Bao, *Nat. Comm.,* **2013**, 5, 3005.

[14] (a) D. Bharti, S. P. Tiwari, *Synt. Metals*, **2016**, *215*, 1. (b) J. Rivnay, L. H. Jimison, J. E. Northrup, M. F. Toney, R. Noriega, S. Lu, T. J. Marks, A. Facchetti, A. Salleo, *Nat. Mat*. **2009**, *8*, 952.

[15] (a) P. Agarwalaa, D. Kabra, *J. Mater. Chem. A*., **2017**, *5,* 1348. (b) J. Wang, K. Liu, L. Ma, X. Zhan, *Chem. Rev*. **2016**, *116*, 14675. (c) O. V. Kozlov, X. Liu, Y. N. Luponosov, A. N. Solodukhin, V. Y. Toropynina, J. Min, M. I. Buzin, S. M. Peregudova, C. J. Brabec, S. A. Ponomarenko, M. S. Pshenichnikov, *J. Phys. Chem. C*., **2017,** *121,* 6424.

[16] (a) Y. Zhao, C. Ye, Y. Qiao, W. Xu, Y. Song, D. Zhu, *Tetrahedron,* **2012**, *68*, 1547. (b) H. Cho, S. Paek, N. Lim, Y. H. Lee, M. K. Nazeeruddin, J. Ko, *Chem. Eur. J.*, **2014**, *20*, 10894. (c) N. Haberkorn, J. S. Gutmann, P. Theato, *ACS nano* , **2009**, *3*(6), 1415,

[17] T. P. I. Saragi, T. F. Lieker, J. Salbeck, *Synthetic Metals*, **2005**, *148*, 267.

[18] M. Sonntag, K. Kreger, D. Hanft, P. Strohriegl, *Chem. Mater*., **2005**, *17*, 3031.

[19] Y. Song, C. Di, W. Xu, Y. Liu, D. Zhanga and D. Zhu, *J. Mater. Chem*., **2007**, *17*, 4483.

[20] (a) A. Cravino, S. Roquet, O. Aleveque, P. Leriche, P. Frere, J. Roncali, *Chem. Mater*., **2006,** *18*, 2584. (b) Y. Song, C. Di, X. Yang, S. Li, W. Xu, Y. Liu, L. Yang, Z. Shuai, D. Zhang, D. Zhu, *J. Am. Chem. Soc.* **2006**, *128*, 15940. (c) P. Devibala, R. Dheepika, P. Vadivelu,.S. Nagarajan , *ChemistrySelec*t, **2019**, *4*, 2339–2346.

[21] R. Dheepika, S. Sonalin, P. M. Imran, S. Nagarajan, *J. Mater. Chem. C,* **2018**, *6*, 6916.

[22] M. S. Liu, X. Jiang, S. Liu, P. Herguth, A. K. Y. Jen, *Macromolecules,* **2002**, *35*, 3532.

[23] (a) G. te Velde, F. M. Bickelhaupt, E. J. Baerends, C. F. Guerra, S. J. A. van Gisbergen J. G. S. T. Ziegler, *Journal of Computational Chemistry*, **2001**, 22(9), 931 (b) G. G. Belmonte, A. Munar, E. M. Barea, J. Bisquert, I. Ugarte, R. Pacios, *Organic Electronics,* **2008**, *9*, 847. (c) S. E. Koh, C. Risko, D. A. S. Filho, O. Kwon, A. Facchetti, J. L. Brédas, T. J. Marks, M. A. Ratner, *Adv. Funct. Mater*. **2008**, *18*, 332

[24] S. H. Wen, W. Q. Deng, K. L. Han, *Phys. Chem. Chem. Phys*., **2010**, *12*, 9267.

[25] C. Quinton, V. A. Rizzo, C. D. Verdes, F. Miomandre, P. Audebert, *Electrochimica Acta*., **2013**, *110*, 693.

[26] J. K. Augustine, A. Bombrun, R. Atta, *Synlett,* **2011**, *15*, 2223.

[27] D. Peckus, T. Matulaitis, M. Franckevius, V. Mimait, T. Tamulevius, J. Simokaitiene, D. Volyniuk, V. Gulbinas, S. Tamulevicius, J. V. Grazulevicius, *J. Phys. Chem. A*, **2018**, *122*(12), 3218.

[28] P.S.Kalsi, *Spectroscopy of organic compounds*, New Age International, India**.**

[29] B. C. Wanga, H. R. Liaoa, J. C. Chang, L. Chenb, J. T. Yeh, J*ournal of Luminescence*, **2007**, *124*, 333.

[30] K. Y. Chiu, T. X. Su, J. H. Li, T. H. Lin, G. S. Liou, S. H. Cheng, *Journal of Electroanalytical Chemistry*, **2005**, *575*, 95. (b) S. J. Yeh, C. Y. Tsai, C. Y. Huang, G. S. Liou, S. H. Cheng, *Electrochemistry Communications*, **2003**, *5*, 373.

[31] Wang, L. Duan, Q. Tao, W. Peng, J. Chen, H. Tan, R. Yang, W. Zhu, *ACS Appl. Mater. Interfaces*, **2016**, *8*, 30320.

[32] N. Li, Z. Fan, H. Zhao, Y. Quan, Q. Chen, S. Ye, S. Li, Q. Fan, W. Huang, *Dyes and Pigments*, **2016**, *134*, 348.

[33] E. Steiner, P. W. Fowler, R. W. A. Havenith, *J. Phys. Chem. A*, **2002**, *106*, 7048.

[34] R. F. Pined, J. Troughton, M. Planells, S. M. Santos, F. Muhith, G. S. Nichol, S. Haque, T. Watson, N. Robertson, *Phys. Chem. Chem. Phys*. **2018**, *20*, 1252.

[35] G. Krucaite, D. Volyniuk, J. Simokaitiene, S. Grigalevicius, C. Lin, C. M. Shao, C. H. Chang, 2019, 162, 196.

[36] (a) D. Gudeika, A. Bundulis, I. Mihailovs, D. Volyniuk, M. Rutkis, J. V. Grazulevicius, *Dyes and Pigments*, **2017**, *140*, 431. (b) D. C. Huang, J. T. Wu, Y. Z. Fan, G. S. Liou, *J. Mater. Chem. C*, **2017**, *5*, 9370.

10.1002/chem.201903450

[37] D. Choi, P. H. Chu, M. McBride, E. Reichmanis, *Chem. Mater*. **2015**, *27*(12), 4167.

[38] (a) H. Kawaguchi*, IEEE Journal of solid-state circuits*, **2005**, *40*(1), 177. (b) K. J. Baeg, D. Khim , J. Kim, B. D. Yang, M. Kang, S. W. Jung , I. K. You, D. Y. Kim, Y. Y. Noh, *Adv. Funct. Mater*., **2012**, *24*, 5433 (c) S. Y. Lee, D. L. Duong, Q. A. Vu, Y. Jin, P. Kim, and Y. H. Lee, *ACS nano*., **2015**, *9*(9), 9034. (d) G. Yang , C. Di , G. Zhang, J. Zhang, J. Xiang, D. Zhang, D. Zhu, *Adv. Funct. Mater*. **2013**, *23*, 1671.

[39] (a) G. Horowitz, *Adv. Mater*. **1996**, *8*(2), 177. (b) G. Horowitz, *Adv. Mater*., **1998,** *10* (5), 365.

[40] I. McCulloch, A. Salleo, M. Chabinyc, *Science*, **2016**, *352*, 1521.

[41] Z. Li, T. Ye, S. Tang, C. Wang, D. Ma and Z. Li, *J. Mater. Chem. C*, 2015, *3*, 2016-2023.

10.1002/chem.201903450

WILEY-VCH

FULL PAPER

Entry for the Table of Contents

Text for Table of Contents: A series of nitrile substituted triarylamines (TAAs) are reported for organic field effect transistors (OFETs) by solution processing. CN group is introduced to alter twist and tilt angle of triarylamine to reach the unsymmetrical architecture. Devices exhibited distinctive *p*- channel behavior with high charge carrier mobility up to 2.8 $cm^2V^{-1}s^{-1}$ with $10^6/10^7$ $I_{ON/OFF}$ ratio.

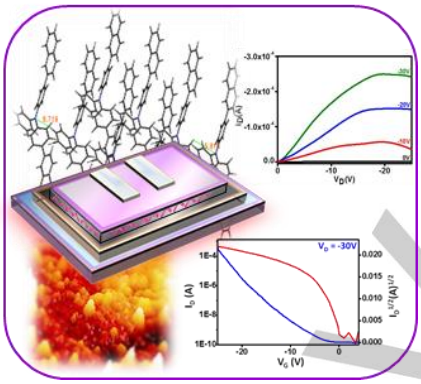

Authors:

Ramachandran Dheepika,[a]
Predhanekar Mohamed Imran,[b]
Nattamai S. P. Bhuvanesh,[c]
*Samuthira Nagarajan**[a]

Title: Solution-processable Unsymmetrical Triarylamines: Towards High Mobility and ON/OFF Ratio in Bottom-gated OFET